BMC Musculoskeletal Disorders

RESEARCH

Open Access

Numerical study of interstitial fluid flow behavior in osteons under dynamic loading

Tianyu Liu[1], Baochuan Xiong[1], Xin Cui[1] and Chunqiu Zhang[1*]

Abstract

Background The porous structure in bone tissue is essential for maintaining the physiological functions and overall health of intraosseous cells. The lacunar-canalicular net (LCN), a microscopic porous structure within osteons, facilitates the transport of nutrients and signaling molecules through interstitial fluid flow. However, the transient behavior of fluid flow within these micro-pores under dynamic loading conditions remains insufficiently studied.

Methods The study constructs a fluid-solid coupling model including the Haversian canal, canaliculi, lacunae, and interstitial fluid, to examine interstitial fluid flow behavior within the LCN under dynamic loading with varying frequencies and amplitudes. The relationship between changes of LCN pore volume and fluid velocity, and pressure is researched.

Results The results demonstrate that increasing strain amplitude leads to significant changes of LCN pore volume within osteons. In a complete loading cycle, with the increase of compressive strain, the pore volume in the osteon gradually shrinks, and the pressure gradient in the LCN increases, which promotes the increase of interstitial fluid velocity. When the compressive strain reaches the peak value, the flow velocity also reaches the maximum. In the subsequent unloading process, the pore volume began to recover, the pressure gradient gradually decreased, the flow rate decreased accordingly, and finally returned to the steady state level. At a loading amplitude of 1000 με, the pore volume within LCN decreases by 1.1‰. At load amplitudes of 1500 με, 2000 με, and 2500 με, the pore volume decreases by 1.6‰, 2.2‰ and 2.7‰ respectively, and the average flow velocity at the center of the superficial lacuna is 1.36 times, 1.77 times, and 2.14 times that at 1000 με, respectively. Additionally, at a loading amplitude of 1000 με under three different loading frequencies, the average flow velocities at the center of the superficial bone lacuna are 0.60 μm/s, 1.04 μm/s, and 1.54 μm/s, respectively. This indicates that high-frequency and high-amplitude dynamic loading can promote more vigorous fluid flow and pressure fluctuations with changes in LCN pore volume.

Conclusions Dynamic mechanical loading can significantly enhance the interstitial fluid flow in LCN by the changes of LCN pore volume. and dynamic loading promoted fluid flow in shallow lacunae significantly higher than that in deep lacunae. The relationship between changes of LCN pore volume and interstitial fluid flow behavior has implications for drug delivery and bone tissue engineering research.

Keywords Dynamic mechanical loading, Lacunar-canalicular system, Interstitial fluid flow, Bone remodeling, Strain amplitude and frequency

*Correspondence:
Chunqiu Zhang
Zhang_chunqiu@126.com

[1]Tianjin Key Laboratory for Advanced Mechatronic System Design and Intelligent Control, School of Mechanical Engineering, Tianjin University of Technology, Tianjin 300384, P.R. China

Introduction

Bone tissue features a unique porous structure composed of cancellous and cortical bone (as shown in Fig. 1). Cortical bone consists of tightly arranged cylindrical units, which have a central hollow area known as the Haversian canal [1, 2]. Surrounding the Haversian canal are elliptical lacunae that house osteocytes [3]. These lacunae are connected to the Haversian canal through micro-channels called canaliculi, which facilitate the exchange of nutrients and metabolites [4]. Collectively, these elements form the lacunar-canalicular net (LCN), a microscopic porous network [5, 6]. The LCN is filled with interstitial fluid rich in ions, nutrients, signaling molecules, and proteins, which are crucial for maintaining the normal physiological functions of bone cells and the overall health of bone tissue [7–9]. In addition to nutrient delivery, the interstitial fluid regulates the response of osteocytes to various physiological and pathological conditions, playing a key role in bone remodeling [10, 11].

The flow of interstitial fluid within the LCN is influenced by circulatory pressure and mechanical loading [12]. When the bone undergoes slight deformation under pressure, changes in the pore volume of the LCN alter interstitial fluid flow behavior. This accelerates the transmission of signaling molecules, promotes the activation of osteoblasts, and enhances the deposition of the bone matrix [13]. Bone cells, recognized as mechanoreceptors in bone tissue, play a crucial role in bone metabolism and remodeling [14–16]. The interstitial fluid flow within the LCN significantly impacts bone cell mechanosensation. The fluid shear forces exerted on bone cells can reorganize their cytoskeleton, changing cell morphology and adhesion properties, and influencing cell division, migration, and physiological functions [17–19]. This shear force is a direct pathway through which bone cells sense mechanical stimuli [20]. For osteoblasts, appropriate shear forces enhance osteogenic activity by increasing the production and mineralization of bone matrix proteins [21]. It also regulates osteoclast activity, influencing the bone resorption process. Additionally, the interstitial fluid flow within the LCN affects the metabolism and signaling molecule transmission in bone cells [22, 23] Therefore, understanding the flow behavior of interstitial fluid in the LCN and its influencing factors is crucial for comprehending the physiological and pathological processes of bones.

The flow of interstitial fluid within the LCN is a complex microscopic process involving various physical parameters and interactions with surrounding tissues [24]. Due to the limitations of microscopic scale and observational techniques, directly observing fluid behavior within the LCN is challenging. Consequently, current research methods primarily utilize finite element analysis and numerical simulation [25–27]. Finite element analysis enables researchers to construct detailed computational models that simulate and analyze these intricate interactions using mathematical and physical approaches, thus providing deeper insights into the flow mechanisms. Wu XG conducted extensive studies on interstitial fluid flow within the LCN under different conditions, developing porous elastic osteon models for various loads. His findings indicate that external load-induced strain significantly affects interstitial fluid pressure [28], and the frequency and amplitude of strain loads can alter fluid flow behavior [29]. Additionally, different loading methods can result in varying interstitial

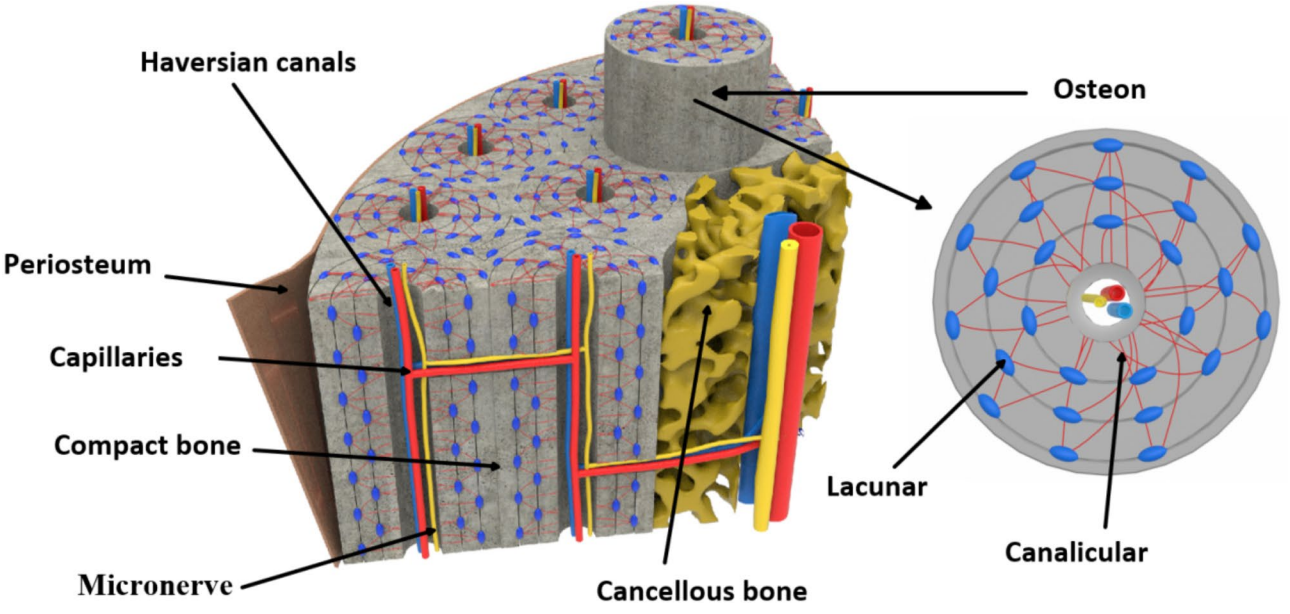

Fig. 1 Microscopic Structure of an Osteon

fluid velocity and pressure distributions [30]. Studies have shown that exposure to microgravity in space causes osteoporosis in astronauts [31]. Our research group hypothesizes that microgravity-induced osteoporosis may be influenced by reduced efficiency of interstitial fluid transport within the LCN [32–34]. When bone tissue is subjected to different gravitational fields, the flow behavior of interstitial fluid within the LCN changes, which subsequently affects bone cell physiology and gene expression. Experiments involving the dynamic perfusion of fluorescent tracer solutions in fluorescence intensity within lacunae under different perfusion pressures and frequencies. These findings highlight the complex interactions between interstitial fluid flow characteristics and the bone cell environment under varying gravitational conditions.

The flow and mass transfer of interstitial fluid within the micro-pore structure of the bone matrix is influenced by various factors [35–37]. The bone matrix consists of osteons, which contain secondary mass transfer channels formed by Haversian canals and the canaliculi-lacunae net. Recent studies have investigated the behavior of interstitial fluid flow in osteons under different gravitational fields, leading to the development of several osteon models. Wu et al. [38] created a model of fluid flow within the canaliculi based on the porous elastic properties of osteons, considering two boundary conditions: elastic and rigid displacement constraints on the osteon's outer wall. Their findings showed that fluid flow and shear stress within the canaliculi are proportional to the strain load's amplitude and frequency. Wang et al. [39] used a multi-scale modeling approach, combining a porous elastic finite element model with a single LCN unit model to study the effects of various loading parameters (such as strain amplitude, strain rate, and cycle number), revealing that strain amplitude and frequency significantly influence fluid velocity and shear stress within the LCN. Fan et al. [25] reconstructed a complete 3D model of the mouse tibia using micro-CT images and predicted the load-driven fluid pressure field using a biphasic porous elastic analysis platform. Joukar [40] developed a single bone cell model and analyzed fluid flow behavior around the bone cell under different loading conditions. Mertiya [51] developed a poromechanical finite element model to study bone tissue's pore pressure, fluid velocity, and mechanobiological stimulus under loading waveforms of different physiological exercises, highlighting running's potential in preventing bone loss and contributing to orthopedic research. Srivas [52] developed a poromechanical model of bone and discovered that the amount of interstitial fluid flow in osteoporotic bone tissue is significantly lower than in healthy bone tissue. Moreover, the fluid in osteoporotic bone is nearly static.

Previous studies have established the relationship between mechanical loading and fluid flow behavior in the LCN. However, the transient behavior of fluid flow within the microchannels of osteons by the changes of LCN pore volume remains insufficiently explored. This paper investigates the transient interstitial fluid flow within the LCN of osteons under dynamic loading. Aiming to provide a foundation for further studies on mechanobiological responses in the bone microstructure. Specifically, this research seeks to clarify how strain amplitude and frequency regulate fluid flow in lacunae and canaliculi by the change of pore volume in osteons, to achieve this, we analyze the relationship between the change in osteon pore volume and transient fluid behavior under dynamic loading.

Model and boundary conditions

Human bones are subjected to various stresses and strains in different environments and during different activities, which are essential for maintaining bone health and functionality [41]. It is well established that dynamic loading has a more significant positive impact on bone remodeling compared to static loading [42]. During daily activities like walking, running, and weight training, bones typically experience strains between 1000 and 2500 microstrain (με). This strain range is considered beneficial for maintaining bone mass. Research indicates that the average strain on bones during daily activities varies with the type of exercise, ranging from approximately 1000 με during walking to 2000 με during jumping [43, 44]. Strains below 100 με can lead to bone resorption, while strains above 3000 με may cause bone damage. Additionally, these activities differ not only in strain amplitude but also in frequency [45, 46]. For instance, the strain frequency is lower during walking but increases with the pace during running [47]. These differences in strain and frequency result in distinct fluid flow behaviors within the LCN. Understanding these mechanisms is crucial for advancing bone science, rehabilitation medicine, and sports biology, as it helps elucidate how complex mechanical stresses impact bone health.

To investigate the interstitial fluid flow behavior within the LCN under dynamic cyclic loading, we developed an osteon model featuring secondary pore structures (see Fig. 2-a). The central blue cylinder represents the Haversian canal, the red dots indicate the lacunae and the green and purple tubes connecting them simulate the transverse and longitudinal canaliculi, respectively. These canaliculi form a dense network, facilitating the efficient transmission of nutrients and signaling molecules between bone cells. Due to the symmetrical structure of the osteon around its central axis, the flow behavior in the horizontal cross-section is also symmetrical. Therefore, a simplified model based on the geometric features

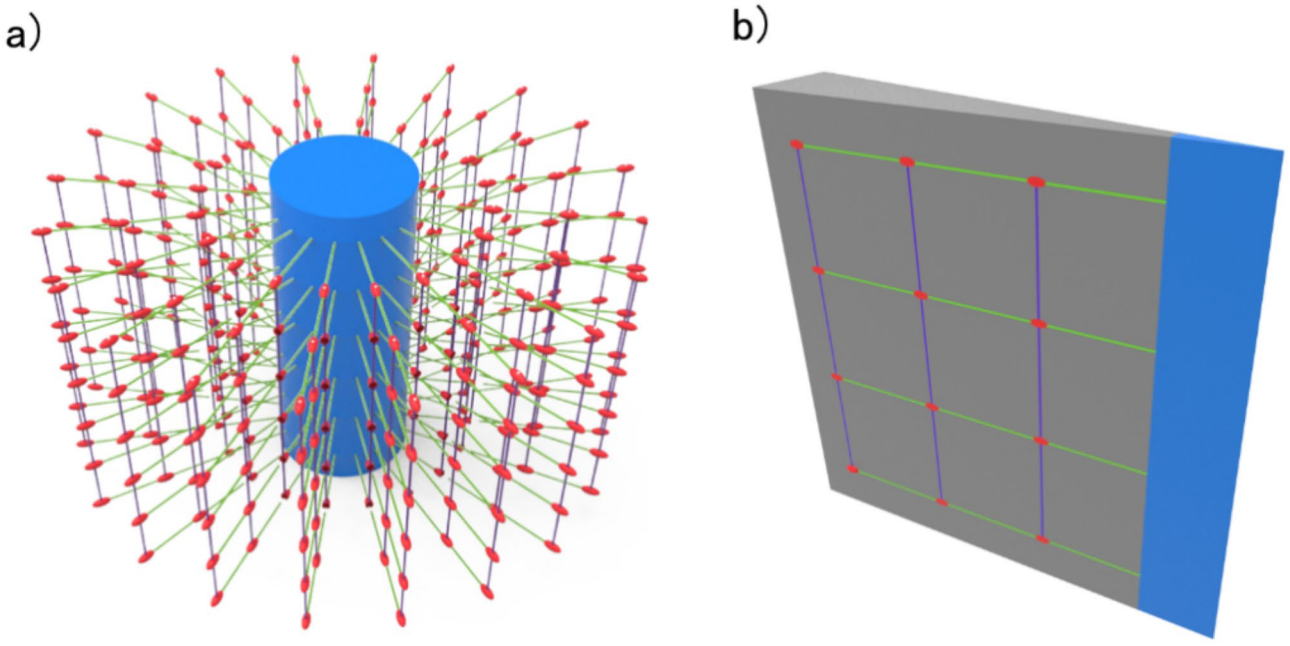

Fig. 2 Osteon Model

of the LCN on one side of the longitudinal section was used for simulation studies (see Fig. 2-b).

To facilitate the quantitative study of pore structures within osteons during cyclic loading, the center of the lacuna was designated as the observation point for pressure and flow velocity. The lacunae and canaliculi under study were grouped and named accordingly. As shown in the figure, the longitudinal canaliculi and lacunae were categorized into three groups: S (shallow), M (middle), and D (deep). The transverse canaliculi were classified as Y1, Y2, and Y3, representing the upper, middle, and lower layers, respectively. Probes were placed at the junctions between these groups and the Haversian canal to monitor the flow velocity of interstitial fluid entering the canaliculi groups. This setup enabled a detailed quantitative analysis of interstitial fluid flow behavior in the canaliculi and lacunae at various depths and heights. It provided insights into the flow characteristics and pressure variations of interstitial fluid at different positions during the cyclic loading period, offering crucial experimental evidence and theoretical support for understanding the fluid flow mechanisms within osteons (Fig. 3).

To explore the behavior of interstitial fluid flow in the LCN under cyclic loading, a series of sinusoidal loa were performed on the osteon model, varying both frequency and amplitude (see Fig. 4). In one set of simulations, the loading amplitudes were 1000 με, 1500 με, 2000 με, and 2500 με at a frequency of 1 Hz. In another set, the loading frequencies were 1 Hz, 2 Hz, and 3 Hz at a fixed amplitude of 1000 με. The top of the Haversian canal was designated as the inlet for interstitial fluid with a pressure of 100 Pa, while the bottom was set as an open boundary. Cyclic displacement loading was applied to the top of the model, with fixed constraints at the bottom-left corner and roller support constraints on the adjacent three surfaces, simulating realistic physical boundary conditions (see Fig. 4a).

This setup mimicked the subtle deformation responses of a micro-osteon during macroscopic bone deformation, preventing necking during stretching and ensuring the authenticity and reliability of the results. The bone matrix was modeled as an isotropic linear elastic material with an elastic modulus of 16.5 GPa and a Poisson's ratio of 0.38. The interstitial fluid was defined as an incompressible fluid with a density of 1080 kg/m^3 and a dynamic viscosity of 0.001 Pa·s. The simulation duration was set to 2 s, covering two complete loading cycles.

To study the response characteristics of osteons under different loading frequencies and amplitudes, a complete sinusoidal loading cycle was divided into compression and stretch phases. Significant time points on the loading curve were identified and numbered. As shown in Fig. 5, the cycle consists of two distinct phases: the compression phase and the stretch phase. P1 and P5 represent the start and end of the cycle, respectively, while P3 corresponds to the point of peak strain. P2 and P4 are the midpoints of the compression and stretch phases, respectively, where the second derivative of the loading curve equals zero, indicating the points of maximum strain rate.

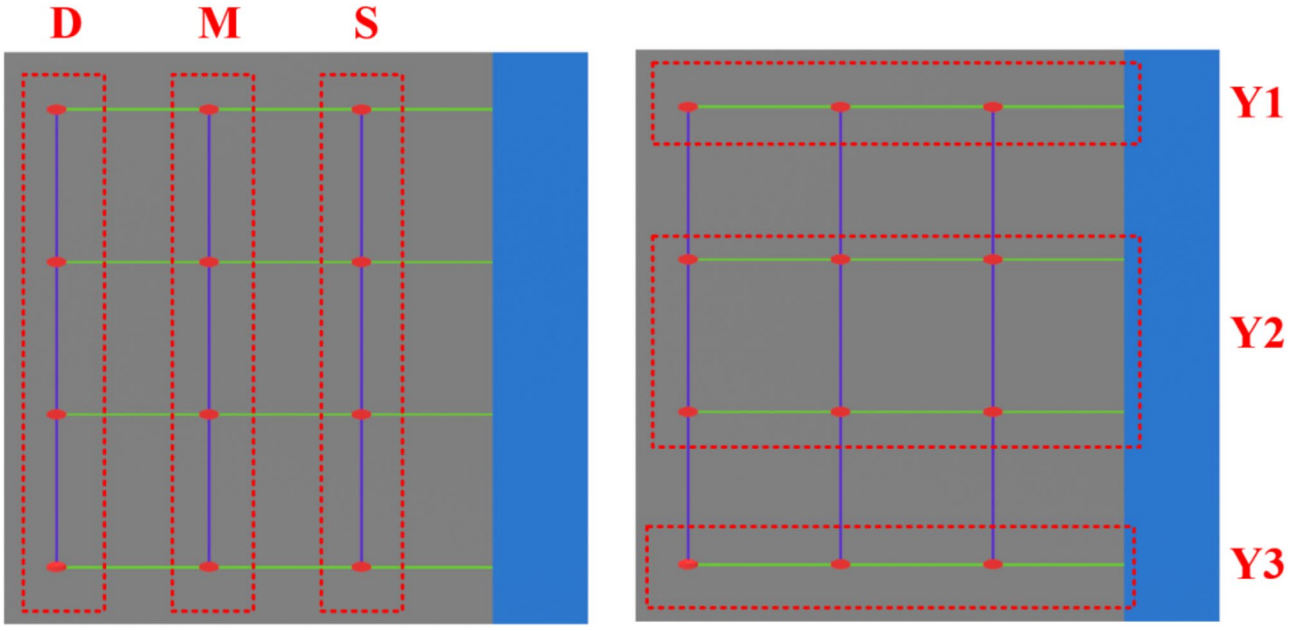

Fig. 3 Classification and Naming of Lacunae and Canaliculi within the LCN

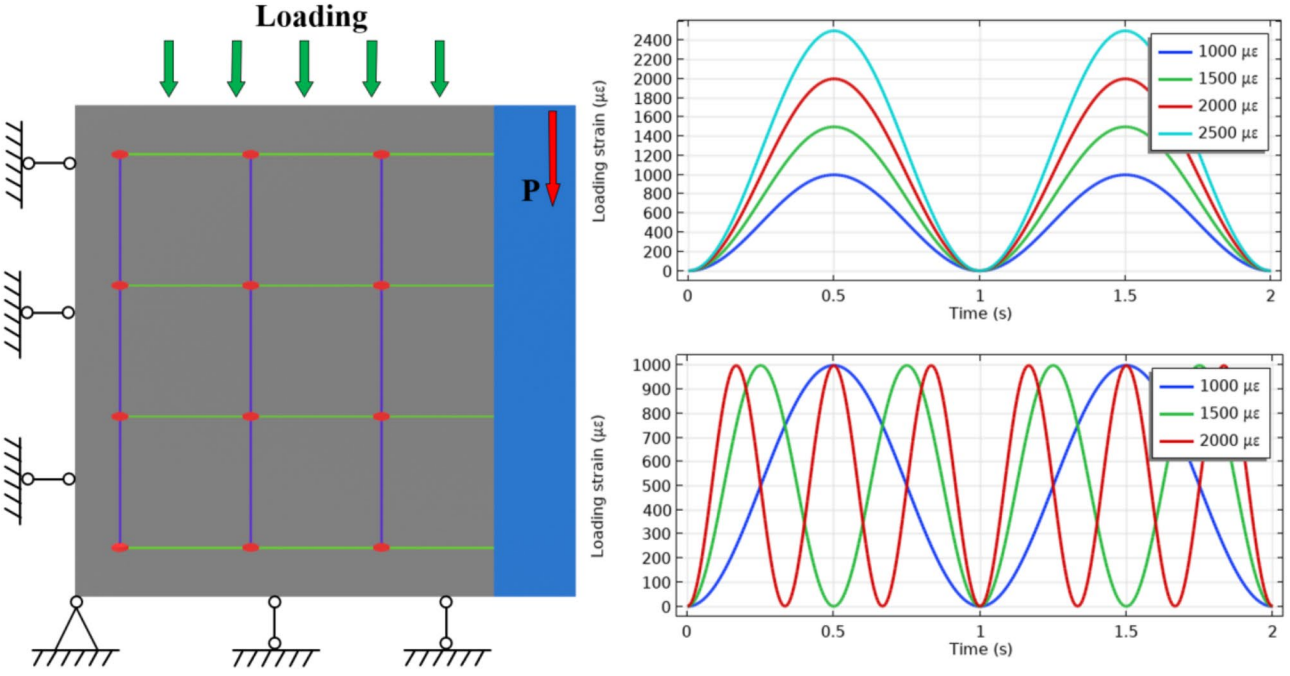

Fig. 4 Boundary Conditions and Strain Driving Function of the Osteon

Result

Different strain amplitudes significantly impact the flow of interstitial fluid (see Fig. 6-a). During cyclic strain loading, the volume of the LCN pore structure in the osteon changes continuously (see Fig. 6-b), influencing the flow behavior of interstitial fluid within the LCN. Simulations of interstitial fluid flow under various loading amplitudes show that increased strain amplitudes boost the flow velocity at the center of the bone lacuna. At a loading amplitude of 1000 με, the average flow velocity at the center of the superficial bone lacuna (S) is 0.585 μm/s. When the loading amplitudes are 1500 με, 2000 με, and 2500 με, the average flow velocity at the center of the superficial bone lacuna increases to 1.36, 1.77, and 2.14 times that at 1000 με, respectively. The enhancement of flow velocity by strain amplitude is approximately linear, with the most significant effect observed in the superficial layer (S). The

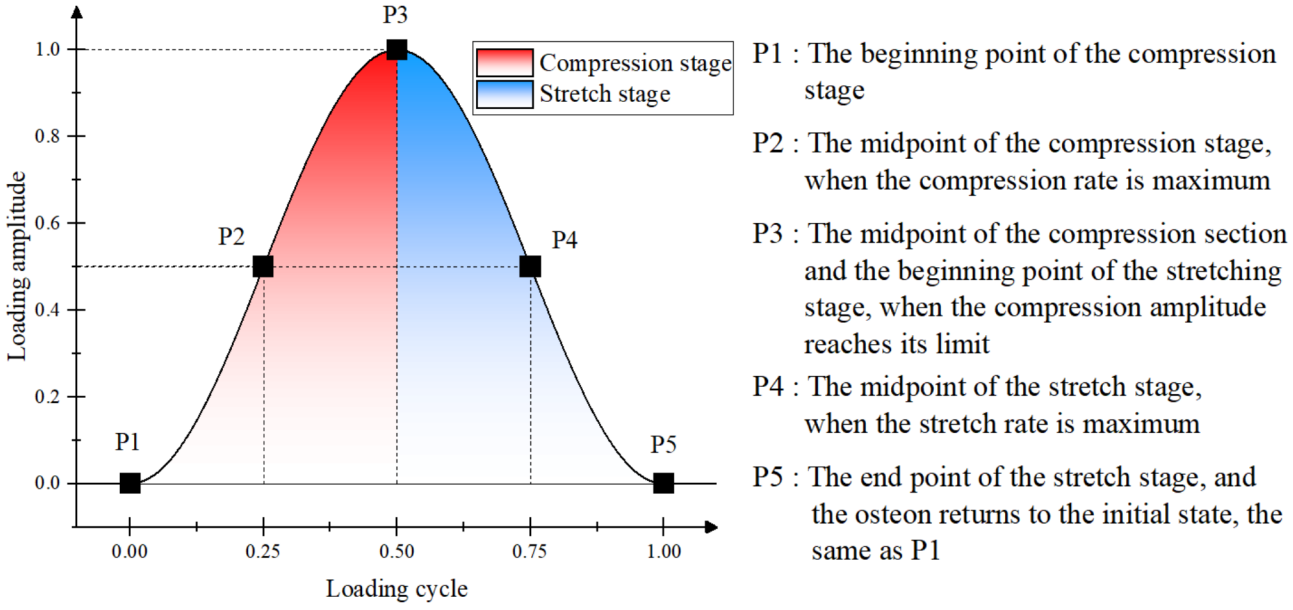

Fig. 5 Strain Phase and Key Point Division During Loading Cycle of Osteon

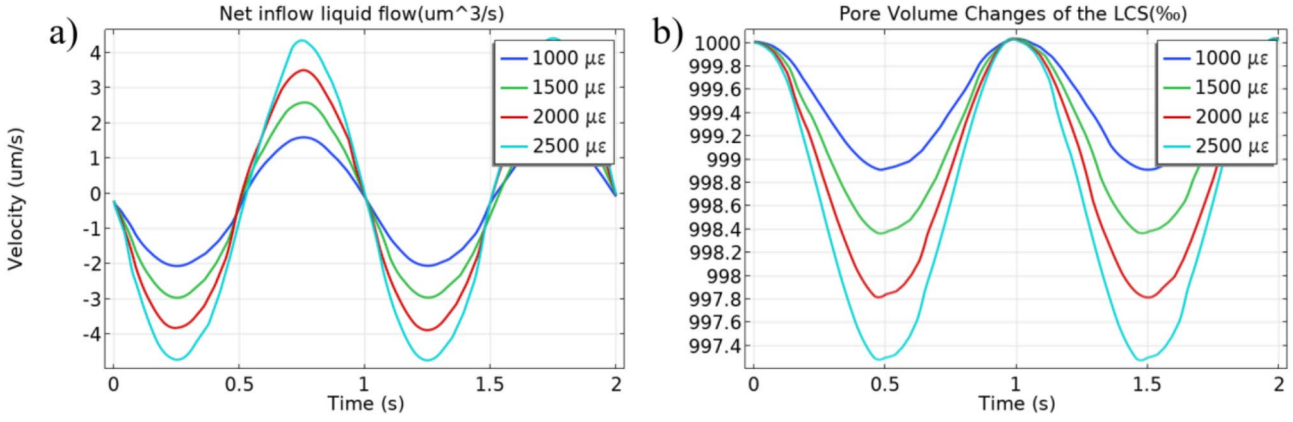

Fig. 6 (**a**) Net Inflow of Fluid in LCN (**b**) Pore Volume Change of LCN

same strain amplitude increases the flow velocity in the middle (M) and deep (D) bone lacunae to 82% and 69% of the effect in the superficial layer (S), respectively.

The flow velocity within the bone lacunae is highly sensitive to loading frequency. For the superficial (S) lacunae, the average flow velocities are 0.60 μm/s, 1.04 μm/s, and 1.54 μm/s at loading frequencies of 1 Hz, 2 Hz, and 3 Hz, respectively. This trend is also evident in the middle (M) and deep (D) bone lacunae. The average flow velocity in the middle lacunae increases from 0.45 μm/s at 1 Hz to 0.82 μm/s at 2 Hz and to 1.26 μm/s at 3 Hz. Similarly, in the deep lacunae, the average flow velocity rises from 0.30 μm/s at 1 Hz to 0.68 μm/s at 2 Hz and to 1.08 μm/s at 3 Hz. Higher loading frequencies intensify the fluid flow within the bone microstructure, driving more interstitial fluid through the LCN during each cycle. This observation aligns with the experimental results of Jing et al. [53]. This increased flow velocity can also enhance the fluid shear stress around bone cells, impacting their biological responses and functions, including cell signaling and matrix protein synthesis [54, 55] (Figure 7).

Analysis of interstitial fluid flow in the LCN under different loading amplitudes

Increasing the strain amplitude significantly enhances the flow of interstitial fluid in the LCN. Observations of the canaliculi and lacunae regions show that the pressure and flow velocity in these areas exhibit sinusoidal changes over time (Fig. 8-a). At a loading strain of 1000 με, the average pressure in the LCN ranges from 23.5 Pa to 77.4 Pa. As the strain amplitude increases, the pressure range expands. When the strain amplitude reaches 1500 με, the minimum pressure becomes negative, and the maximum pressure exceeds the preset inlet pressure

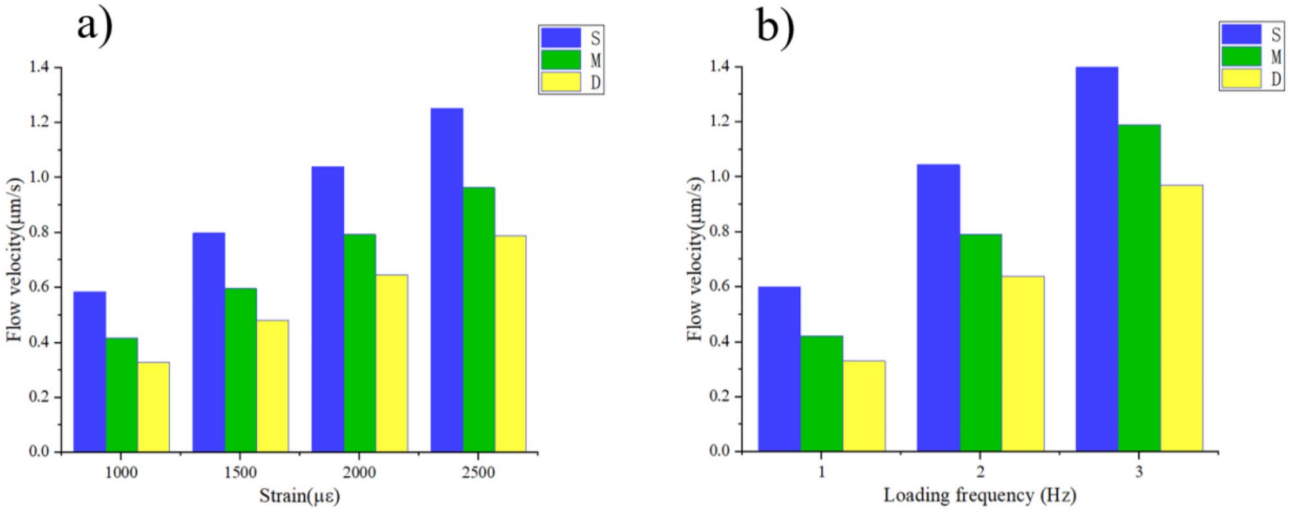

Fig. 7 (**a**) Flow Velocity at the Center of Bone Lacunae under Different Strain Amplitudes (**b**) Flow Velocity at the Center of Bone Lacunae under Different Loading Frequencies

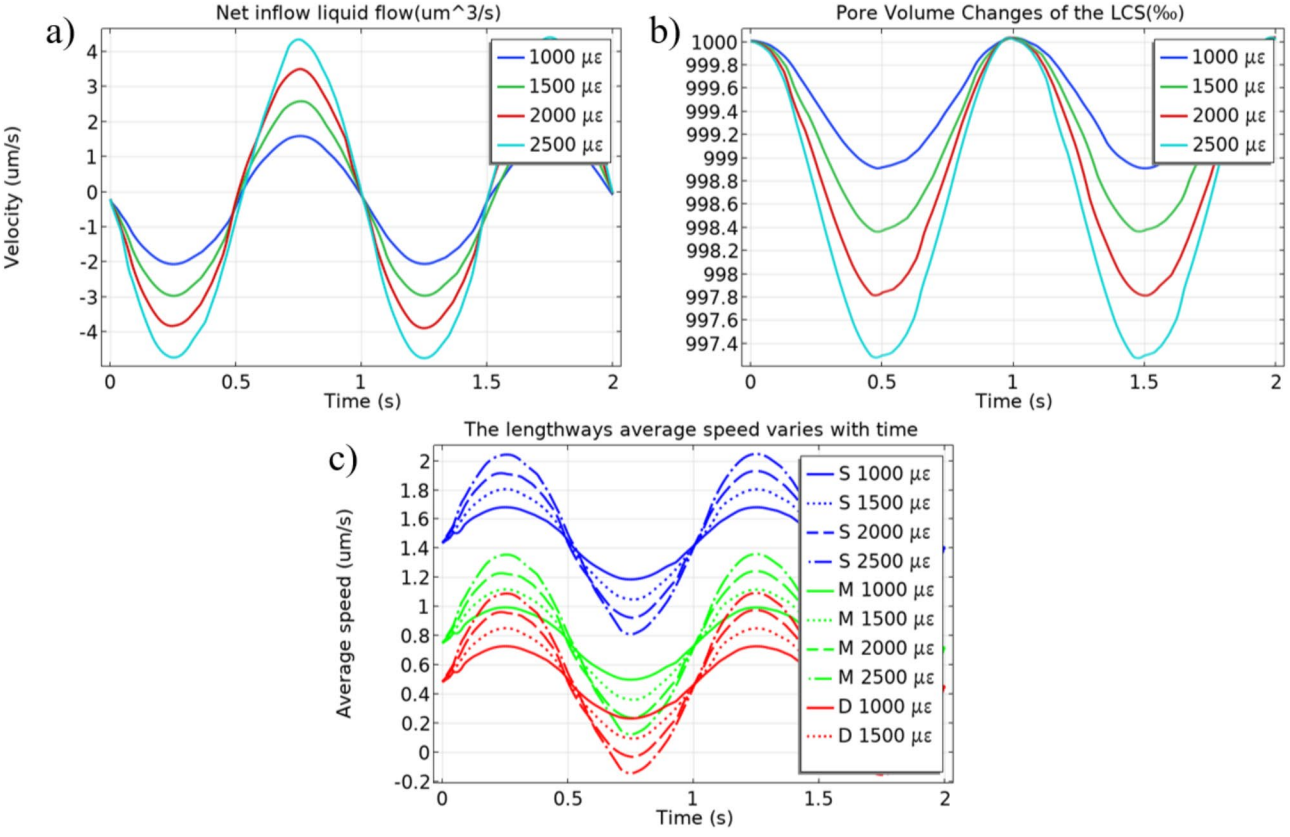

Fig. 8 (**a**)Average Pressure Variation with Time.(**b**)Average Speed Variation with Time. (**c**) Lengthways Average Speed Variation with Time

(100 Pa). This effect becomes more pronounced with increasing strain amplitude, resulting in more drastic pressure changes over time.

The minimum and maximum pressures occur at P2 and P4 on the loading curve, indicating that the volume change rate of the osteon peaks at these points, causing negative or overpressure in the LCN and promoting interstitial fluid inflow and outflow. This inference is supported by the time-varying data of average flow velocity in the LCN (Fig. 8-b). The direction of interstitial fluid outflow from the LCN is defined as positive. When the osteon is compressed, the pore volume decreases,

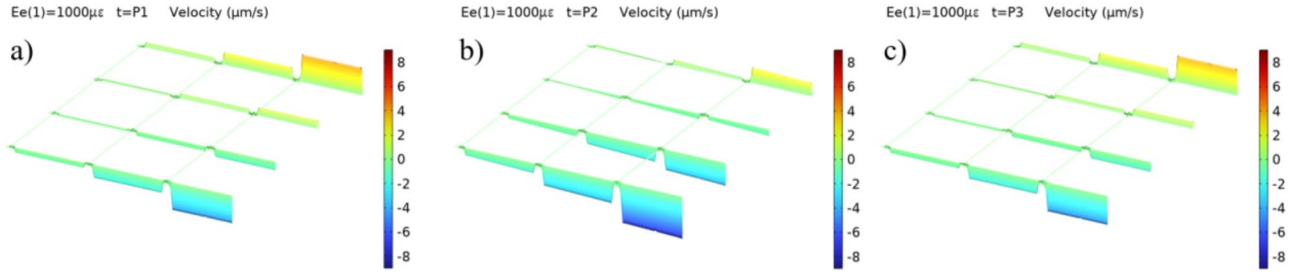

Fig. 9 Transverse Canaliculi Flow Velocity Distribution During Compression Stage Over Time (**a**) t = P1; (**b**) t = P2; (**c**) t = P3

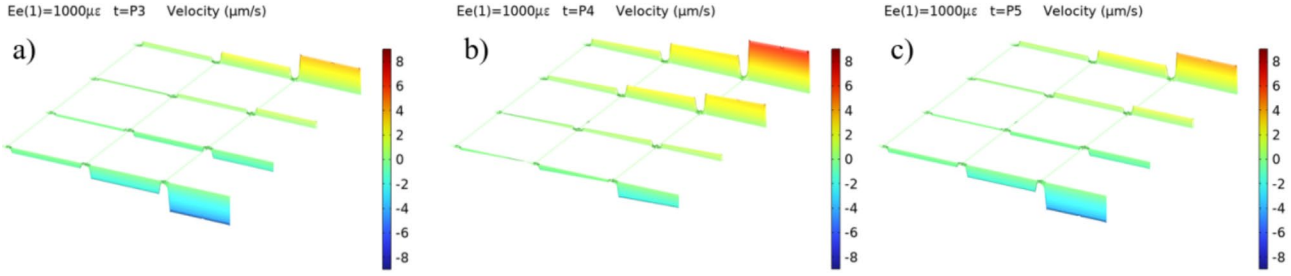

Fig. 10 Transverse Canaliculi Flow Velocity Distribution During Stretch Phase Over Time (**a**) t = P3; (**b**) t = P4; (**c**) t = P5

increasing the pressure and flow velocity in the LCN, thereby squeezing out the interstitial fluid. Conversely, as the load decreases and the volume restores, negative pressure is generated in the LCN, driving interstitial fluid into it.

Furthermore, the flow velocity of interstitial fluid varies across different longitudinal canaliculi groups (Fig. 8-d). While the promoting effect of loading amplitude is consistent across all depth layers (S, M, D), the flow velocity in deep canaliculi is generally lower than in superficial ones. Due to higher flow resistance in the deep LCN, reverse flow can occur in the D-layer canaliculi, leading to a lower capacity for solute transport in the interstitial fluid and potentially limiting the osteon diameter to 150–300 μm.

The time-dependent distribution of flow velocity within the LCN (as shown in Fig. 9) provides a clearer view of interstitial fluid behavior under cyclic loading. Defining the inflow direction of interstitial fluid into the LCN as positive, Fig. 9 illustrates the flow velocity distribution at three time points during the compression phase of the osteon.

At t = P1 (Fig. 9-a), when the strain rate is 0 με/s, the flow velocity distribution follows a steady-state pattern, with interstitial fluid entering from Y1 and exiting through Y3, exhibiting symmetrical flow velocities. At t = P2 (Fig. 9-b), the strain rate reaches 1000 με/s, significantly increasing the flow velocity in the Y3 group. At this point, the pore volume in the LCN decreases, and the interstitial fluid outflow rate reaches its maximum. At t = P3 (Fig. 9-c), the strain rate drops back to zero, and the flow velocity distribution returns to the steady-state pattern.

During the stretching phase of the osteon, the flow velocity distribution in the transverse canaliculi is similar to that during compression (as shown in Fig. 10). However, at t = P4 (when the stretching rate is at its peak), the flow velocity distribution reverses compared to the stretching phase. As the pore volume of the LCN increases, a large amount of interstitial fluid flows in from Y1, while the flow velocity in Y3 nearly drops to zero. This phenomenon indicates that under sinusoidal cyclic strain loading, the flow velocity of interstitial fluid in the LCN also exhibits sinusoidal fluctuations. During this process, the pore volume of the LCN continually changes, alternately drawing in and expelling interstitial fluid, the study by Fu et al. [57] also reached the same conclusion.

Under sinusoidal cyclic loading with the same frequency, higher loading amplitudes result in higher peak flow velocities in the canaliculi (Fig. 11). Comparing the peak flow velocity distribution in the transverse canaliculi of the LCN at different loading amplitudes, it is evident that at a loading amplitude of 1000 με, the Y3 group reaches its peak flow velocity when the osteon's compression rate is highest, while the flow velocity in the Y1 group exhibits an opposite trend. As the loading amplitude increases, the flow velocity in the Y1 canaliculi decreases. At a loading amplitude of 2500 με, the flow direction in the Y1 canaliculi aligns with that in the Y3 group. This occurs because higher loading amplitudes at the same frequency induce greater volume change rates in the osteon, resulting in more intense pressure

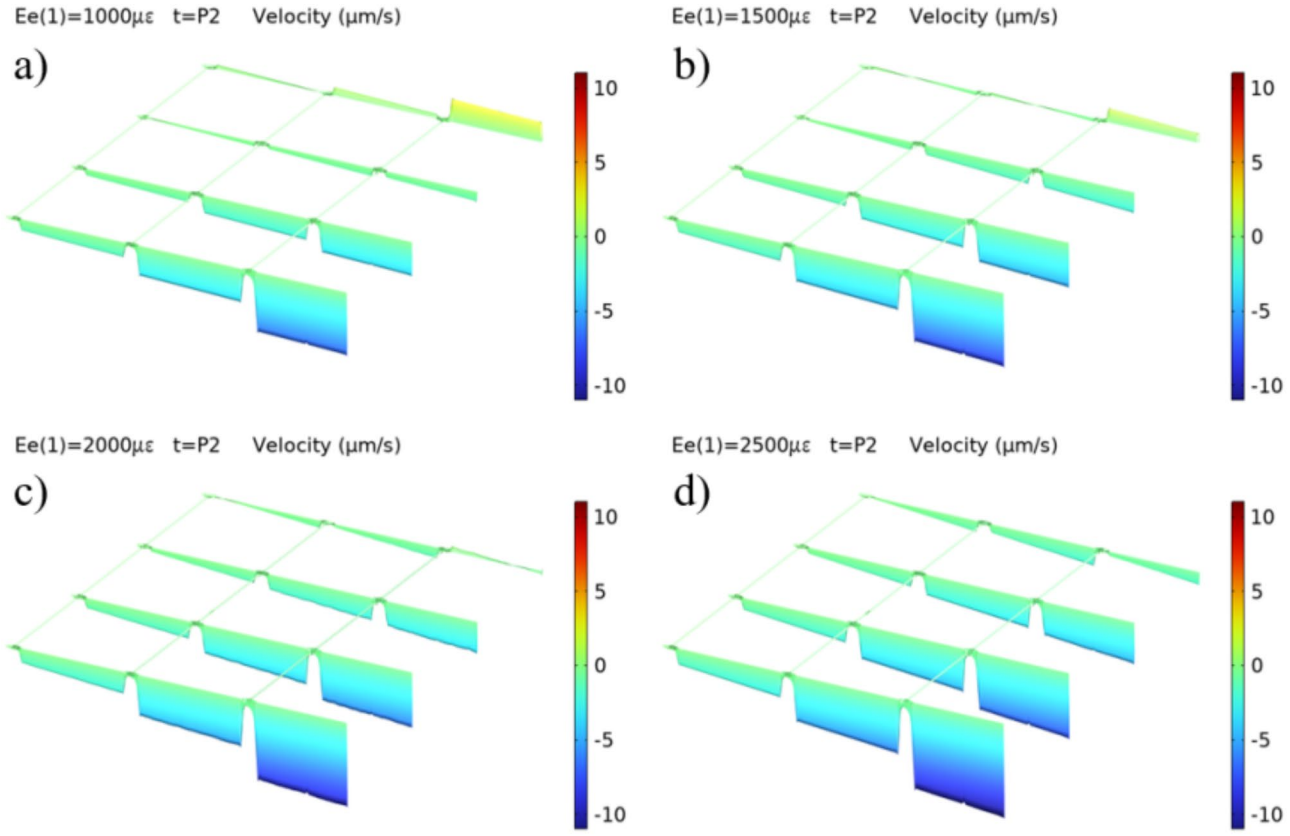

Fig. 11 Peak Flow Velocity in Transverse Canaliculi Under Different Loading Amplitudes (**a**) 1000 με; (**b**) 1500 με; (**c**) 2000 με; (**d**) 2500 με

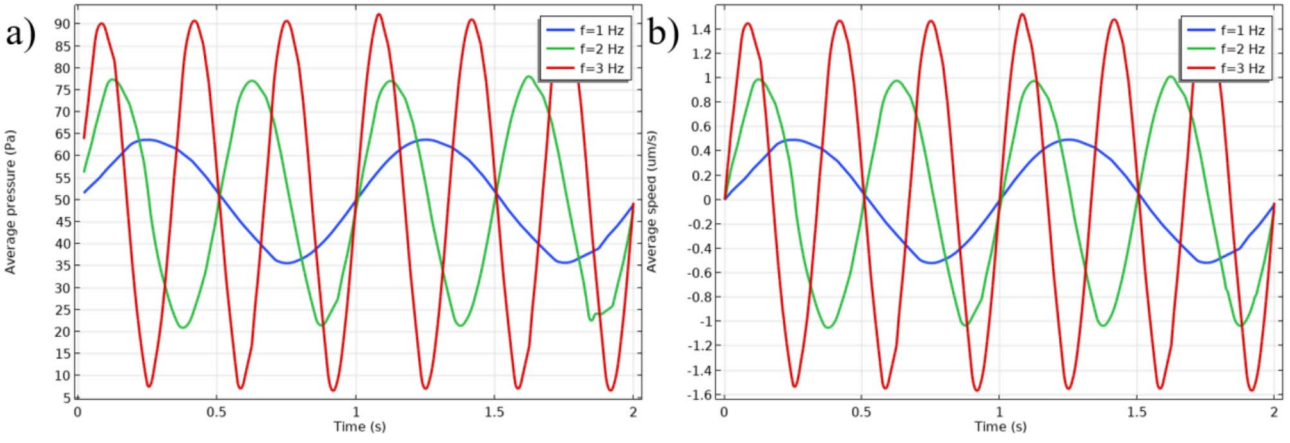

Fig. 12 Average Pressure(**a**) and Flow Velocity(**b**) in LCN Under Different Loading Frequencies

variations within the LCN and, consequently, more vigorous fluid flow driven by the pressure gradient.

Analysis of interstitial fluid flow in the LCN under different loading frequencies

Under dynamic cyclic loading with an amplitude of 1000 με and frequencies of 1 Hz, 2 Hz, and 3 Hz, loading frequency significantly impacts the flow of interstitial fluid in the LCN. At a loading frequency of 1 Hz, the peak average pressure in the LCN is 77.5 Pa. This peak increases to 105 Pa at 2 Hz and 133 Pa at 3 Hz, with peak strain rates of 2000 με/s and 3000 με/s, respectively. The peak average flow velocity in the LCN also shows a linear increase with loading frequency (Fig. 12). Higher loading frequencies cause the osteon to deform more rapidly, creating a greater pressure gradient that raises the peak flow velocity of the interstitial fluid [56].

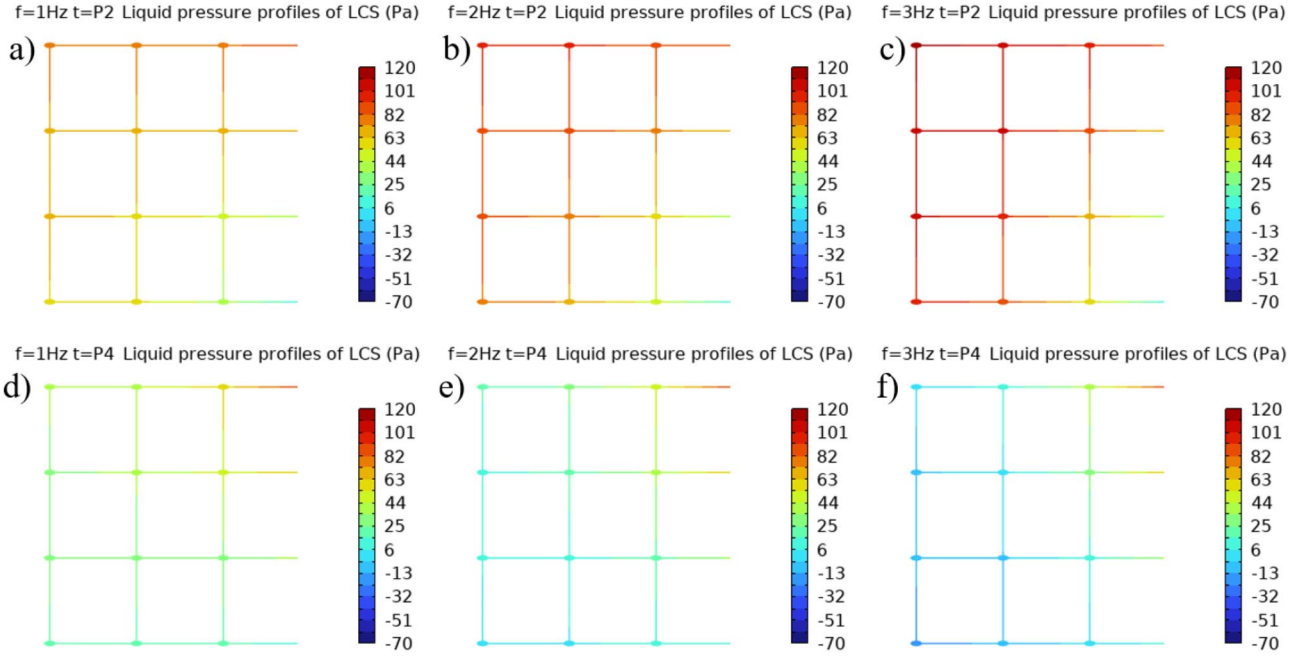

Fig. 13 LCN Pressure Distribution at Midpoints of Compression and Stretch Phases Under Different Loading Frequencies. (**a**) f = 1 Hz, t = P2 (**b**) f = 2 Hz, t = P2 (**c**) f = 3 Hz, t = P2 (**d**) f = 1 Hz, t = P4 (**e**) f = 1 Hz, t = P4 (**f**) f = 1 Hz, t = P4

As shown in Fig. 13, at a loading frequency of 1 Hz, the maximum pressure difference within the LCN is approximately 85 Pa, with all points maintaining positive pressure. However, as the loading frequency increases, negative pressure begins to appear deep within the LCN, and the pressure difference widens. At frequencies of 2 Hz and 3 Hz, the maximum pressure differences increase to 122 Pa and 160 Pa, respectively. This widening pressure difference drives faster interstitial fluid flow.

Conclusion

This study developed a fluid-solid coupled microscopic model of an osteon incorporating the LCN system to examine the characteristics of interstitial fluid flow under dynamic strain loading by changs of LCN pore volume within osteons. The flow behavior of interstitial fluid within the LCN exhibits periodic changes. During the stretching and compression phases, the flow velocity distribution follows symmetrical patterns, with both the frequency and amplitude of the dynamic loading significantly influencing the interstitial fluid flow. Increasing the loading amplitude and frequency leads to a notable rise in the flow velocity within the LCN. This is attributed to the higher rates of volume change in the osteon, resulting in alternating negative and positive pressures deep within the LCN. These rapid volume changes generate more substantial pressure gradients, driving the interstitial fluid to flow at higher velocities within the LCN. Furthermore, mechanical loading has a greater impact on promoting fluid flow in the superficial layers of the LCN than in the deeper layers.

Discussion

In this study, a fluid-solid coupling-based lacunar-canalicular system (LCN) network model of the osteon was constructed to analyze fluid flow behavior under dynamic loading. The interstitial fluid velocity and pressure within the LCN fluctuate significantly with changes in the rate of mechanical loading, following a pattern similar to the loading curve. Bone cells, functioning as mechanoreceptors, demonstrate increased osteogenic activity and enhanced matrix protein synthesis under high fluid shear forces [48–50]. The high fluid shear forces observed in our simulations help to understand the mechanobiological responses of bone cells. Conversely, lower amplitude and frequency loading may not provide enough mechanical stimulation, leading to reduced bone cell activity, bone loss, or impaired bone remodeling. This mechanism is crucial for explaining the mass transfer behavior and cellular responses of bone tissue under varying mechanical loads. Additionally, higher fluid velocities in the LCN, driven by rapid loading rates, promote the exchange of essential nutrients, signaling molecules, and the removal of metabolic waste, which is necessary for bone cell growth, this result implies that for the group of osteoporosis patients who are not suitable for high-intensity rehabilitation training, external intervention with low-intensity and high-frequency dynamic stimulation may be a more ideal choice strategy. The fluid velocity in

superficial canaliculi and lacunae is more sensitive to mechanical loading changes, meaning that increased mechanical loading does not significantly enhance fluid flow in the deeper LCN layers. As the osteon diameter increases, the fluid stimulation effect on deeper lacunae diminishes, potentially explaining why individual osteon diameters typically range between 150 and 300 μm. The findings of this study have important theoretical and practical implications for understanding bone cell behavior under dynamic loading. By precisely controlling loading conditions, we can simulate bone tissue responses under various physiological and pathological states in vitro, providing new research directions and therapeutic strategies for osteoporosis, fracture healing, and bone tissue engineering.

However, this study has some limitations. Firstly, it used a sinusoidal curve to simulate mechanical loading conditions similar to physiological activities, while in reality, human activities involve various and more complex loading scenarios. Additionally, the study did not fully account for other factors that could influence the fluid dynamics within the LCN, such as variations in bone density across different parts of the body and differences in the lacunar-canalicular system between individuals of different ages. Furthermore, it should be noted that this model has not yet been experimentally validated. Although the simulation results align with trends reported in the existing literature, the practical applicability and accuracy of the model remain subject to further verification and optimization due to limitations in experimental conditions. Future research should integrate experimental methods to systematically validate the assumptions and results of the model, thereby enhancing its credibility and practical application value.

Future research should investigate the effects of various types of dynamic loads, such as multiaxial and asymmetric impact loads, on interstitial fluid flow within the LCN and bone cell responses. This includes examining processes such as cell signaling, nutrient transport, and waste removal. By simulating the movement of particles and molecules within the LCN, researchers can gain deeper insights into how mechanical loads influence bone cell metabolism. Integrating experimental validation with multiscale modeling will enable a more comprehensive understanding of the multi-level mechanisms through which mechanical loads affect bone tissue, thereby advancing the fields of bone science, rehabilitation medicine, and biomechanics.

Acknowledgements
Not applicable.

Author contributions
TYL conducted the finite element simulations and was a major contributor in writing the manuscript. BCX conducted the literature review. XC organized and analyzed the simulation data. CQZ reviewed and approved the final manuscript. All authors read and approved the final manuscript.

Funding
This study was supported by National Natural Science Foundation of China (12072235).

Data availability
The datasets used and/or analysed during the current study are available from the corresponding author on reasonable request.

Declarations

Ethics approval and consent to participate
Not applicable.

Consent for publication
Not applicable.

Competing interests
The authors declare no competing interests.

Received: 7 August 2024 / Accepted: 13 February 2025
Published online: 24 February 2025

References

1. Enlow DH. Functions of the Haversian system. 1962.
2. Burr DB. Bone morphology and organization, in Basic and applied bone biology. Elsevier; 2019. pp. 3–26.
3. Bonucci E. Basic composition and structure of bone. Mechanical testing of bone and the bone-implant interface. Boca Raton: CRC; 2000. pp. 3–21.
4. Ullah R et al. Alveolar Bone, in An Illustrated Guide to Oral Histology. 2021. pp. 99–121.
5. Liu H-Y, et al. Research on solute transport behaviors in the lacunar-canalicular system using numerical simulation in microgravity. Comput Biol Med. 2020;119:103700.
6. Zhang C, et al. Ageing characteristics of bone indicated by transcriptomic and exosomal proteomic analysis of cortical bone cells. J Orthop Surg Res. 2019;14:1–17.
7. DiGirolamo DJ, Kiel DP, Esser KA. Bone and skeletal muscle: neighbors with close ties. J Bone Miner Res. 2013;28(7):1509–18.
8. Karsenty G, Oury F. Biology without walls: the novel endocrinology of bone. Annu Rev Physiol. 2012;74:87–105.
9. DiGirolamo DJ, Clemens TL, Kousteni S. The skeleton as an endocrine organ. Nat Rev Rheumatol. 2012;8(11):674–83.
10. Hernandez-Gil IF-T, et al. Physiological bases of bone regeneration I. Histology and physiology of bone tissue. Med Oral. 2006;11(1):47–51.
11. Hart NH, et al. Biological basis of bone strength: anatomy, physiology and measurement. J Musculoskel Neuronal Interact. 2020;20(3):347.
12. Weinbaum S, Cowin SC, Zeng Y. A model for the excitation of osteocytes by mechanical loading-induced bone fluid shear stresses. J Biomech. 1994;27(3):339–60.
13. Cowin SC. Bone poroelasticity. J Biomech. 1999;32(3):217–38.
14. Franz-Odendaal TA, Hall BK, Witten PE. Buried alive: how osteoblasts become osteocytes. Dev Dynamics: Official Publication Am Association Anatomists. 2006;235(1):176–90.
15. Bonewald LF. Osteocytes as dynamic multifunctional cells. Ann N Y Acad Sci. 2007;1116(1):281–90.
16. Burger EH, Klein-Nulend J. Mechanotransduction in bone—role of the lacunocanalicular network. FASEB J. 1999;13(9001):S101–12.
17. Sun Y, et al. Mechanical stimulation on mesenchymal stem cells and surrounding microenvironments in bone regeneration: regulations and applications. Front cell Dev Biology. 2022;10:808303.
18. Yavropoulou MP, Yovos J. The molecular basis of bone mechanotransduction. J Musculoskel Neuronal Interact. 2016;16(3):221.
19. Ferrara B, et al. The extracellular matrix in pancreatic cancer: description of a complex network and promising therapeutic options. Cancers. 2021;13(17):4442.

20. Jin J, et al. Physicochemical niche conditions and mechanosensing by osteocytes and myocytes. Curr Osteoporos Rep. 2019;17:235–49.
21. Sun W, et al. The mechanosensitive Piezo1 channel is required for bone formation. Elife. 2019;8:e47454.
22. Lai X, et al. Lactation alters fluid flow and solute transport in maternal skeleton: a multiscale modeling study on the effects of microstructural changes and loading frequency. Bone. 2021;151:116033.
23. Ahn AC, Grodzinsky AJ. Relevance of collagen piezoelectricity to Wolff's Law: a critical review. Med Eng Phys. 2009;31(7):733–41.
24. Zhao S et al. Fluid-solid coupling numerical simulation of entire rat caudal vertebrae under dynamic loading. Comput Methods Biomech BioMed Eng, 2024: pp. 1–10.
25. Fan L, et al. A multiscale 3D finite element analysis of fluid/solute transport in mechanically loaded bone. Bone Res. 2016;4(1):1–10.
26. Liu H-Y, et al. Simulation study on the effect of resistance exercise on the hydrodynamic microenvironment of osteocytes in microgravity. Comput Methods Biomech BioMed Eng. 2022;25(15):1757–66.
27. Deligianni D, Apostolopoulos C. Multilevel finite element modeling for the prediction of local cellular deformation in bone. Biomech Model Mechanobiol. 2008;7(2):151–9.
28. Wu X, et al. The effects of haversian fluid pressure and harmonic axial loading on the poroelastic behaviors of a single osteon. Volume 55. Science China Physics, Mechanics and Astronomy; 2012. pp. 1646–56.
29. Wu X, et al. Mathematically modeling fluid flow and fluid shear stress in the canaliculi of a loaded osteon. Biomed Eng Online. 2016;15:261–73.
30. Wu X-G, et al. Interstitial fluid flow behavior in osteon wall under non-axisymmetric loading: a finite element study. J Mech Med Biology. 2018;18(07):1840007.
31. Cariati I, et al. Recombinant irisin prevents cell death and mineralization defects induced by random positioning machine exposure in primary cultures of human osteoblasts: a promising strategy for the osteoporosis treatment. Front Physiol. 2023;14:1107933.
32. Wang H, et al. Study on mass transfer in the bone lacunar-canalicular system under different gravity fields. J Bone Miner Metab. 2022;40(6):940–50.
33. Wang H, et al. The lack of mass transfer in bone lacunar-canalicular system may be the decisive factor of osteoporosis under microgravity. Life Sci Space Res. 2021;31:80–4.
34. Wang H, et al. Numerical simulation on mass transfer in the bone lacunar-canalicular system under different gravity fields. Comput Methods Biomech BioMed Eng. 2024;27(4):478–88.
35. Keanini RG, Roer RD, Dillaman RM. A theoretical model of circulatory interstitial fluid flow and species transport within porous cortical bone. J Biomech. 1995;28(8):901–14.
36. Kaiser J. Bone mechanotransduction: interstitial fluid flow, microstructure and biochemical coupling. 2011, Université Paris-Est.
37. Smit TH. Finite element models of osteocytes and their load-induced activation. Curr Osteoporos Rep. 2022;20(2):127–40.
38. Wu X-G, et al. Hierarchical model for strain generalized streaming potential induced by the canalicular fluid flow of an osteon. Acta Mech Sin. 2015;31(1):112–21.
39. Wang H, et al. Interactive effects of various loading parameters on the fluid dynamics within the lacunar-canalicular system for a single osteocyte. Bone. 2022;158:116367.
40. Joukar A, Niroomand-Oscuii H, Ghalichi F. Numerical simulation of osteocyte cell in response to directional mechanical loadings and mechanotransduction analysis: considering lacunar–canalicular interstitial fluid flow. Comput Methods Programs Biomed. 2016;133:133–41.
41. Carter DR. Mechanical loading histories and cortical bone remodeling. Calcif Tissue Int. 1984;36(Suppl 1):S19–24.
42. Forwood MR, et al. Increased bone formation in rat tibiae after a single short period of dynamic loading in vivo. Am J Physiology-Endocrinology Metabolism. 1996;270(3):E419–23.
43. Burr DB, et al. In vivo measurement of human tibial strains during vigorous activity. Bone. 1996;18(5):405–10.
44. Lanyon L, et al. Bone deformation recorded in vivo from strain gauges attached to the human tibial shaft. Acta Orthop Scand. 1975;46(2):256–68.
45. Turner CH, Pavalko FM. Mechanotransduction and functional response of the skeleton to physical stress: the mechanisms and mechanics of bone adaptation. J Orthop Sci. 1998;3:346–55.
46. Duncan RL, Turner CH. Mechanotransduction and the functional response of bone to mechanical strain. Calcif Tissue Int. 1995;57:344–58.
47. Kohrt WM, et al. Physical activity and bone health. Med Sci Sports Exerc. 2004;36(11):1985–96.
48. Xu H, et al. Oscillatory fluid flow elicits changes in morphology, cytoskeleton and integrin-associated molecules in MLO-Y4 cells, but not in MC3T3-E1 cells. Biol Res. 2012;45(2):163–9.
49. Verbruggen SW, Vaughan TJ, McNamara LM. Fluid flow in the osteocyte mechanical environment: a fluid–structure interaction approach. Biomech Model Mechanobiol. 2014;13(1):85–97.
50. Stewart S, et al. Mechanotransduction in osteogenesis. Bone Joint Res. 2020;9(1):1–14.
51. Mertiya AS, Tiwari AK, Mishra A, Main RP, Tripathi D. Tiwari Biomech Model Mechanobiol 22 (1), 281–95.
52. Shrivas NV, Tiwari AK, Kumar R, Patil S, Badhyal S. (2021). Physiological loading-induced interstitial fluid dynamics in osteon of osteogenesis imperfecta bone. J Biomech Eng, 143(8).
53. Jing D, D Baik A, L Lu X, Zhou B, E Guo X. In situ intracellular calcium oscillations in osteocytes in intact mouse long bones under dynamic mechanical loading. FASEB J. 2013;28(4):1582–92.
54. Zhou CPX, Li W, Wang L. Real-time measurement of solute transport within the lacunar-canalicular system of mechanically loaded bone:Direct evidence for load-induced fluid flow, Journal of Bone and Mineral Research, Volume 26, Issue 2, 1 February 2011, Pages 277–285.
55. Wei F, Flowerdew K, Kinzel M, et al. Changes in interstitial fluid flow, mass transport and the bone cell response in microgravity and normogravity. Bone Res. 2022;10:65. https://doi.org/10.1038/s41413-022-00234-9.
56. Zhao S, Chen Z, Li T, Sun Q, Leng H, Huo B. Numerical simulations of fluid flow in trabecular–lacunar cavities under cyclic loading. Computers in Biology and Medicine; 2023. p. 163.
57. Fu R. December, Haisheng Yang; Effects of lacunocanalicular morphology and network architecture on fluid dynamic environments of osteocytes and bone mechanoresponses. Physics of fluids 1 2024; 36 (12): 121915.

Publisher's note